

## Vacancy defects in electron-irradiated ZnO studied by Doppler broadening of annihilation radiation

Z. Q. Chen,<sup>1,\*</sup> K. Betsuyaku,<sup>2</sup> and A. Kawasuso<sup>3</sup>

<sup>1</sup>Hubei Nuclear Solid Physics Key Laboratory, Department of Physics, Wuhan University, Wuhan 430072, People's Republic of China

<sup>2</sup>Science Solution Division, Mizuho Information and Research Institute, Inc., 2-3, Kanda-Nishikicho, Chiyoda-ku, Tokyo 101-8443, Japan

<sup>3</sup>Advanced Science Research Center, Japan Atomic Energy Agency, 1233 Watanuki, Takasaki, Gunma 370-1292, Japan

(Received 17 February 2008; published 14 March 2008)

Vacancy defects in ZnO induced by electron irradiation were characterized by the Doppler broadening of annihilation radiation measurements together with the local density approximation calculations. Zinc vacancies ( $V_{\text{Zn}}$ ) are responsible for positron trapping in the as-irradiated state. These are annealed out below 200 °C. The further annealing at 400 °C results in the formation of secondary defects attributed to the complexes composed of zinc vacancies and zinc antisites ( $V_{\text{Zn}}\text{-Zn}_{\text{O}}$ ).

DOI: 10.1103/PhysRevB.77.113204

PACS number(s): 61.72.J-, 71.55.Gs, 78.70.Bj

Due to the wide band gap and large exciton binding energy, ZnO has attracted much attention in recent years.<sup>1</sup> Interests in ZnO were focused on the  $p$ -type doping, nanostructures growth, and ferromagnetic properties. However, relatively little attention was paid to intrinsic defects despite their important roles in the electric and optical properties. The self-compensation of intrinsic defects could cause difficulty in  $p$ -type doping.<sup>2</sup> They also degrade the ultraviolet emission process by acting as nonradiative recombination centers. Recently, it is found that some intrinsic defects can be even responsible for the ferromagnetism.<sup>3,4</sup>

There are still many fundamental problems concerning intrinsic defects in ZnO. For example, the candidate for the unintentional  $n$ -type conductivity is still controversial. Oxygen vacancies ( $V_{\text{O}}$ ) or zinc interstitials ( $\text{Zn}_i$ ) have long been suggested to act as native donors.<sup>5,6</sup> However, more recent calculation by Janotti and Van de Walle<sup>7</sup> showed that both  $V_{\text{O}}$  and  $\text{Zn}_i$  have high formation energies. The origin of the green luminescence in ZnO is also under debate. It has been correlated with various defects, such as  $V_{\text{O}}$ ,  $V_{\text{Zn}}$ ,  $\text{Zn}_i$ , oxygen antisites ( $\text{O}_{\text{Zn}}$ ), and even Cu impurities.<sup>7-11</sup> The reason for the above problems lies in the difficulty in unambiguously identifying those defects.

Positron annihilation is an established tool in the study of defects in semiconductors because of its superb sensitivity to vacancy-type defects. Positrons are preferentially trapped by vacancy defects. The positron annihilation characteristics such as positron lifetime and the Doppler broadening of annihilation radiation (DBAR) are modulated by vacancy defects due to the reduced electron density and the change of electron momentum distribution.

There have been a few newly published positron annihilation studies on ZnO.<sup>12-16</sup> Recently, we reported about vacancy defects in electron-irradiated ZnO.<sup>15</sup> We obtained an intriguing result indicating the formation of secondary defects after the disappearance of  $V_{\text{Zn}}$  and  $V_{\text{O}}$ . However, no further identification of the secondary defects could be made. In this Brief Report, to identify the observed defect species in electron-irradiated ZnO, we examined the experimental coincidence DBAR spectra and compared with the theoretical calculation for various defects.

Hydrothermal-grown  $n$ -type ZnO(0001) single crystals from Scientific Production Company (SPC goodwill) were irradiated with 3 MeV electrons to a dose of  $5.5 \times 10^{18} e^-/\text{cm}^2$  keeping the temperature below 70 °C. Postirradiation annealing was conducted from 100 to 700 °C in  $\text{N}_2$  atmosphere with a duration of 30 min. Chemical-vapor-transportation-grown ZnO single crystals from Eagle Pitcher Industry were used as the reference samples because they have the highest quality among our samples. A positron source was prepared by depositing  $^{22}\text{NaCl}$  ( $3.7 \times 10^5$  Bq) onto titanium thin films with 5  $\mu\text{m}$  thick. Positron lifetime measurements were carried out using a conventional spectrometer with a time resolution of 210 ps. The DBAR measurements were performed in both single and coincidence modes using the high purity Ge detectors with energy resolutions of 1.3 at 511 keV. In the coincidence mode,  $3 \times 10^7$  counts were accumulated. The positron lifetime spectra were analyzed using PATFIT-88 program.<sup>17</sup> Single-detector DBAR spectra were characterized by  $S$  and  $W$  parameters, which are defined as the normalized intensities of the central ( $511 \pm 0.85$  keV) and tail ( $511 \pm 3.4$ – $511 \pm 6.8$  keV) regions of the spectra, respectively. Two-dimensional data obtained in the coincidence DBAR measurements were projected onto the  $E_1$ – $E_2$  ( $=2\Delta E$ ) axis. A window of  $1022 - 2.6$  keV  $< E_1 + E_2 < 1022 + 2.6$  keV along the diagonal was chosen to remove any irrelevant noisy signals. A symmetric one-dimensional DBAR spectrum was then obtained with peak to background ratio of  $10^5$ . The Doppler energy shift of  $\Delta E = 1$  keV corresponds to the longitudinal momentum  $p_L = 3.92 \times 10^{-3} m_0 c$ .

The DBAR spectra for bulk ZnO and various defect states were calculated within the local density approximation,<sup>18</sup>

$$\rho(\mathbf{p}) = \pi r_e c^2 \sum_n \left| \int e^{-i\mathbf{p}\cdot\mathbf{r}} \Psi_+(\mathbf{r}) \Psi_n(\mathbf{r}) \sqrt{\gamma(\mathbf{r})} d\mathbf{r} \right|^2, \quad (1)$$

where  $r_e$  is the classical electron radius,  $c$  is the speed of light,  $\Psi_+(\mathbf{r})$  is the positron wave function,  $\Psi_n(\mathbf{r})$  is the  $n$ th state electron wave function, and  $\gamma(\mathbf{r})$  is the enhancement factor. For the valence electrons, the summation was performed over all the occupied band. For the core electrons,

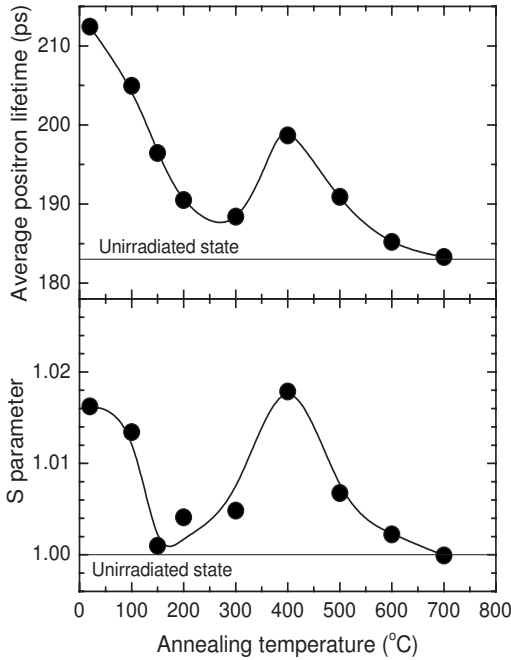


FIG. 1. Average positron lifetime and  $S$  parameter as a function of annealing temperature obtained from 3 MeV electron-irradiated ZnO to a dose of  $5.5 \times 10^{18} e^-/\text{cm}^2$ . The annealing duration was 30 min.

$\Psi_n(\mathbf{r})$  is represented by  $\Psi_{i,nlm}(\mathbf{r}-\mathbf{R}_i)$ , where  $(nlm)$  are the principal, azimuthal and magnetic quantum numbers for the  $i$ th atom and  $\mathbf{R}_i$  denotes the position vector.<sup>19</sup>

The valence electron wave functions were calculated based on the projector augmented-wave method<sup>20</sup> using the ABINIT4.6.4 code.<sup>21</sup> The potentials and projectors were generated using the ATOMPAW code.<sup>22</sup> For Zn and O atoms, the valence electron configurations were  $3d^{10}4s^2$  and  $2s^22p^4$ , respectively. A supercell including four Zn and four O atoms was constructed for the perfect lattice. For the defect structures, the supercell includes 32 Zn and 32 O atoms, and relevant atoms were removed and/or replaced. The lattice constants were fixed to be  $a=3.25 \text{ \AA}$  and  $c=5.21 \text{ \AA}$ .<sup>23</sup> The  $k$ -point grid was  $2 \times 2 \times 2$  for the perfect lattice. Only the  $\Gamma$  point was considered for the defect structures. The lattice relaxations around defects were considered based on the molecular dynamics simulation implemented in the ABINIT code. The cut-off energy of the plane wave basis set was 60 Ry. The core electron wave function was represented by the Slater function parametrized by Clementi and Roetti.<sup>24</sup> A self-consistent positron wave function was calculated based on the two-component density functional theory in order to minimize the energy functional.<sup>25</sup> The Boroński–Nieminen enhancement factor was adopted.<sup>25</sup> The DBAR spectra were obtained by convoluting one-dimensional angular correlation of annihilation radiation spectra obtained from  $\rho(\mathbf{p})$  with the Gaussian resolution function having the half width of  $3.92 \times 10^{-3} m_0 c$ .

Figure 1 shows the annealing behavior of the average positron lifetime and  $S$  parameter in ZnO after electron irradiation reported in our previous paper.<sup>15</sup> The single lifetime in the unirradiated state is approximately 183 ps. No defect

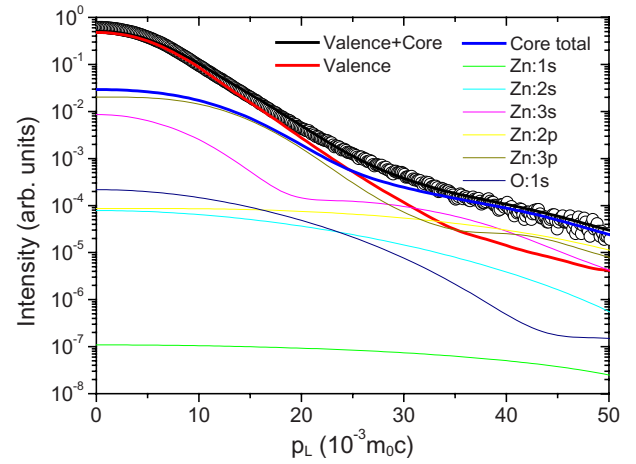


FIG. 2. (Color online) Open circles denote the DBAR spectrum in the coincidence mode obtained from the reference ZnO sample. Solid lines are the calculated DBAR curves.

components were obtained. After irradiation, the average lifetime increased to 212 ps. The second lifetime component with a value of 230 ps related to vacancy defects was obtained. The  $S$  parameter also increased to 1.016 after irradiation. It was inferred that  $V_{\text{Zn}}$  are responsible for positron trapping since positrons are not well localized at  $V_{\text{O}}$ . As shown in Fig. 1, most vacancy defects disappeared after annealing below 200 °C. However, both lifetime and  $S$  parameter again increased after annealing at 400 °C. Hall measurements revealed no shift of the Fermi level at 400 °C, thus the possibility of charge transition of defects was ruled out. We suggested that some new defect species were generated due to annealing. The  $S$ - $W$  plot also supported this assumption. From the Raman scattering measurements, we observed that  $V_{\text{O}}$  started to recover at 200–400 °C. Considering these results, we suggested two possible defect reactions occurred during annealing:  $V_{\text{O}} \Rightarrow V_{\text{Zn}} + \text{Zn}_{\text{O}}$  and/or  $V_{\text{Zn}} + V_{\text{O}} \Rightarrow V_{\text{Zn}}V_{\text{O}}$ . Thus, either  $V_{\text{Zn}}-\text{Zn}_{\text{O}}$  complexes or  $V_{\text{Zn}}V_{\text{O}}$  divacancies may be the secondary defects in electron-irradiated ZnO. However, we could not confirm these two possibilities. To identify the origin of the above vacancy defects, we examine the detailed electron momentum distributions given by the DBAR in coincidence mode as shown below.

Figure 2 shows the DBAR spectrum in coincidence mode measured for the reference sample (Eagle Pitcher Industry). Solid lines denote the calculated curves. It can be seen that the experimental and theoretical results agree with each other fairly well. At  $p_L < 15 \times 10^{-3} m_0 c$ , the valence electrons contribute most to the spectrum, while at  $p_L > 30 \times 10^{-3} m_0 c$ , core electrons mainly contribute to the momentum distribution. Among the core electrons, contribution from Zn 3p and 3s electrons is predominant and produces a wide distribution.

Figure 3 shows the DBAR spectra in the as-irradiated state and after annealing at 400 °C, which are differentiated by the spectrum for the reference sample  $[N(p_L)/N_R(p_L)]$ . Such “ratio curves” are used to enhance the small differences between two spectra. For the comparison with calculation later, the amplitudes of the above two curves around

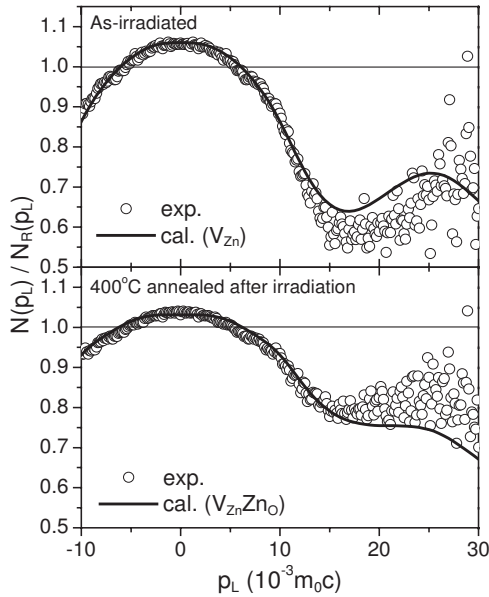


FIG. 3. Open circles denote the DBAR spectra in the coincidence mode obtained from ZnO after 3 MeV electron irradiation to a dose of  $5.5 \times 10^{18} e^-/\text{cm}^2$  and after postirradiation annealing at 400 °C, which are differentiated (ratio) by the spectrum for the reference sample ( $N(p_L)/N_R(p_L)$ ). The solid lines are the calculated ratio curves.

$N(p_L)/N_R(p_L)=1$  are adjusted to 2.2 and 1.6 times, respectively, from their original curves. After irradiation, the intensities of the DBAR spectrum increase and decrease in the low and high momentum regions, respectively. This means that the annihilation probability with electrons having higher momenta relatively decreases at the vicinity of vacancy defects. After annealing at 400 °C, the spectrum becomes a little broader and the intensity in high momentum region ( $p_L > 15 \times 10^{-3} m_0 c$ ) increases as compared to the ratio curve for the as-irradiated state. This again suggests formation of secondary defects shown in Fig. 1.

Figure 4 shows the calculated ratio curves for various defects. The ratio curve for  $V_O$  is nearly independent of  $p_L$ , i.e.,  $N_{\text{defects}}(p_L)/N_{\text{bulk}}(p_L) \sim 1$ . This means that the DBAR curve for  $V_O$  is rather similar to that for the bulk. The reason is that positrons are only weakly localized at  $V_O$  and the annihilation probability with the bulk electrons is predominant. Thus,  $V_O$  is essentially invisible to positrons as suggested in the previous study.<sup>12</sup> Although the difference is not so large, the ratio curve for  $V_O-O_{\text{Zn}}$  changed from that for  $V_O$ . This is because by replacing one of the four Zn atoms surrounding  $V_O$  with an O atom, the positron trapping potential is deepened. Contrary, the amplitudes of the ratio curve for  $V_{\text{Zn}}$  increase in both low and high momentum regions. That for  $V_{\text{Zn}}V_O$  further increases in low momentum region. This indicates that positrons are well localized at these defects. The ratio curve for  $V_{\text{Zn}}-Zn_O$  exhibits a broader feature as compared to those for  $V_{\text{Zn}}$  and  $V_{\text{Zn}}V_O$  in the low momentum region. This is due to an increase in the annihilation probability with Zn 3d electrons by the replacement of the nearest neighbor O sites with Zn atoms.

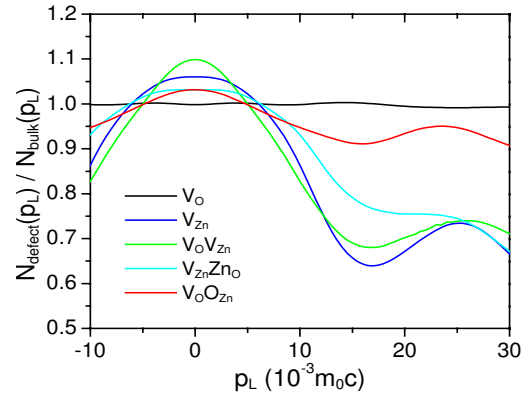


FIG. 4. (Color online) Calculated DBAR spectra for various defects in ZnO that are differentiated (ratio) by the bulk spectrum [ $N_{\text{defect}}(p_L)/N_{\text{bulk}}(p_L)$ ].

The ratio curve in the as-irradiated state is compatible with the calculated one for  $V_{\text{Zn}}$ , as shown by the solid line in Fig. 3. This confirms that  $V_{\text{Zn}}$  are responsible for positron trapping in the as-irradiated state. The ratio curve after annealing at 400 °C is compatible with that for  $V_{\text{Zn}}-Zn_O$ , as shown by the solid line in Fig. 3, and not with those for  $V_{\text{Zn}}$ ,  $V_{\text{Zn}}V_O$ , and  $V_O-O_{\text{Zn}}$ . As can be seen in Fig. 1, most  $V_{\text{Zn}}$  are removed by annealing up to 200 °C, formation of  $V_{\text{Zn}}V_O$  will be unlikely. Therefore, only  $V_O \Rightarrow V_{\text{Zn}}+Zn_O$  could probably reflect the formation process of the secondary defects, i.e.,  $V_O$  transform into  $V_{\text{Zn}}-Zn_O$  complexes through occupation of the  $V_O$  sites with neighboring Zn atoms. We can thus conclude that the secondary defects formed after postirradiation annealing are attributed to  $V_{\text{Zn}}-Zn_O$ .

The decomposed positron lifetime at secondary defects is close to that of  $V_{\text{Zn}}$ , i.e., 230 ps, but with large uncertainty due to the reduced defect concentration. Assuming the same specific positron trapping rate of  $3 \times 10^{15} \text{ s}^{-1}$  as for  $V_{\text{Zn}}$ , the concentration of the secondary defects can be roughly estimated as  $7 \times 10^{16}/\text{cm}^3$ . The Doppler broadening ratio curves also yield the comparable values. These secondary defects are removed at about 700° since all the positron annihilation parameters recover to the unirradiated state, as shown in Fig. 1.

In summary, through the comparison between experimental and calculated DBAR spectra, we confirm that  $V_{\text{Zn}}$  are the primary defects acting as positron trapping centers in the electron-irradiated ZnO, and  $V_{\text{Zn}}-Zn_O$  are the secondary defects formed due to post-irradiation annealing at around 400 °C.

This work was partly supported by the Program for New Century Excellent Talents in University and the National Natural Science Foundation of China under Grants No. 10475062 and No. 10075037. In the positron calculation, we used some resources developed in “Embedded High-Performance Computing (EHPC) Project” supported by Special Coordination Funds for Promoting Science and Technology of MEXT Japan.

\*chenzq@whu.edu.cn

- <sup>1</sup>U. Ozgur, Ya I. Alivov, C. Liu, A. Teke, M. A. Reshchikov, S. Dogan, V. Avrutin, S.-J. Cho, and H. Morkoc, *J. Appl. Phys.* **98**, 041301 (2005).
- <sup>2</sup>Eun-Cheol Lee, Y.-S. Kim, Y.-G. Jin, and K. J. Chang, *Phys. Rev. B* **64**, 085120 (2001).
- <sup>3</sup>W. S. Yan, Z. H. Sun, Q. H. Liu, Z. R. Li, Z. Y. Pan, J. Wang, S. Q. Wei, D. Wang, Y. X. Zhou, and X. Y. Zhang, *Appl. Phys. Lett.* **91**, 062113 (2007).
- <sup>4</sup>Q. Y. Xu, H. Schmidt, L. Hartmann, H. Hochmuth, M. Lorenz, A. Setzer, P. Esquinazi, C. Meinecke, and M. Grundmann, *Appl. Phys. Lett.* **91**, 092503 (2007).
- <sup>5</sup>D. C. Look, J. W. Hemsky, and J. R. Sizelove, *Phys. Rev. Lett.* **82**, 2552 (1999).
- <sup>6</sup>D. C. Look, G. C. Farlow, Pakpoom Reunchan, Sukit Limpijumnong, S. B. Zhang, and K. Nordlund, *Phys. Rev. Lett.* **95**, 225502 (2005).
- <sup>7</sup>A. Janotti and C. G. Van de Walle, *Phys. Rev. B* **76**, 165202 (2007).
- <sup>8</sup>F. K. Shan, G. X. Liu, W. J. Lee, G. H. Lee, I. S. Kim, and B. C. Shin, *Appl. Phys. Lett.* **86**, 221910 (2005).
- <sup>9</sup>T. Moe Borseth, B. G. Svensson, A. Yu. Kuznetsov, P. Klason, Q. X. Zhao, and M. Willander, *Appl. Phys. Lett.* **89**, 262112 (2006).
- <sup>10</sup>B. Lin, Z. Fu, and Y. Jia, *Appl. Phys. Lett.* **79**, 943 (2001).
- <sup>11</sup>N. Y. Garces, L. Wang, L. Bai, N. C. Giles, L. E. Halliburton, and G. Cantwell, *Appl. Phys. Lett.* **81**, 622 (2002).
- <sup>12</sup>Z. Q. Chen, S. Yamamoto, M. Maekawa, A. Kawasuso, X. L. Yuan, and T. Sekiguchi, *J. Appl. Phys.* **94**, 4807 (2003).
- <sup>13</sup>F. Tuomisto, V. Ranki, K. Saarinen, and D. C. Look, *Phys. Rev. Lett.* **91**, 205502 (2003).
- <sup>14</sup>G. Brauer, W. Anwand, W. Skorupa, J. Kuriplach, O. Melikhova, C. Moisson, H. von Wenckstern, H. Schmidt, M. Lorenz, and M. Grundmann, *Phys. Rev. B* **74**, 045208 (2006).
- <sup>15</sup>Z. Q. Chen, S. J. Wang, M. Maekawa, A. Kawasuso, H. Naramoto, X. L. Yuan, and T. Sekiguchi, *Phys. Rev. B* **75**, 245206 (2007).
- <sup>16</sup>A. Zubiaga, F. Plazaola, J. A. Garcia, F. Tuomisto, V. Munoz-Sanjose, and R. Tena-Zaera, *Phys. Rev. B* **76**, 085202 (2007).
- <sup>17</sup>P. Kirkegaard, N. Pederson, and M. Eldrup, *PATFIT-88, Riso-M-2704*, 1989.
- <sup>18</sup>M. J. Puska and R. M. Nieminen, *Rev. Mod. Phys.* **66**, 841 (1994).
- <sup>19</sup>M. Alatalo, B. Barbiellini, M. Hakala, H. Kauppinen, T. Korhonen, M. J. Puska, K. Saarinen, P. Hautojärvi, and R. M. Nieminen, *Phys. Rev. B* **54**, 2397 (1996).
- <sup>20</sup>P. E. Blöchl, *Phys. Rev. B* **50**, 17953 (1994).
- <sup>21</sup>X. Gonze, J.-M. Beuken, R. Caracas, F. Detraux, M. Fuchs, G.-M. Rignanese, L. Sindic, M. Verstraete, G. Zerah, F. Jollet, M. Torrent, A. Roy, M. Mikami, Ph. Ghosez, J.-Y. Raty, and D. C. Allan, *Comput. Mater. Sci.* **25**, 478 (2002).
- <sup>22</sup>N. A. W. Holzwarth, A. R. Tackett, and G. E. Matthews, *Comput. Phys. Commun.* **135**, 329 (2001).
- <sup>23</sup>O. Madelung, *Semiconductors Basic Data* (Springer-Verlag, Berlin, 1996), p. 182.
- <sup>24</sup>E. Clementi and C. Roetti, *At. Data Nucl. Data Tables* **14**, 177 (1974).
- <sup>25</sup>E. Boroński and R. M. Nieminen, *Phys. Rev. B* **34**, 3820 (1986).